CEIG - Spanish Computer Graphics Conference (2013), pp. 1–9
M. Carmen Juan and Diego Borro (Editors)

Rendering Relativistic Effects in Transient Imaging

Adrian Jarabo[1] Belen Masia[1,2] Andreas Velten[2,3] Christopher Barsi[2] Ramesh Raskar[2] Diego Gutierrez[1]

[1]Universidad de Zaragoza [2]MIT Media Lab [3]Morgridge Institute for Research

Abstract

We present a real-time framework which allows interactive visualization of relativistic effects for time-resolved light transport. We leverage data from two different sources: real-world data acquired with an effective exposure time of less than 2 picoseconds, using a novel imaging technique termed femto-photography, and a transient renderer based on ray-tracing. We overcome the two main limitations of existing models for relativistic effects, namely the assumption that surface irradiance is constant over time, and that all frames of reference are purely translational. We explore the effects of time dilation, light aberration, frequency shift and radiance accumulation, as an unconstrained virtual camera explores a reconstructed 3D scene depicting dynamic illumination. We modify existing models of these relativistic effects to take into account the time-resolved nature of our data, and introduce the first model of relativistic sensor rotation in computer graphics.

1. Introduction

Analyzing and synthesizing light transport is a core research topic in computer graphics, computing vision and scientific imaging [GNJJ08]. One of the most common simplifications, rarely challenged, is the assumption that the speed of light is infinite. While this is a valid assumption in most cases, it is certainly not true: light travels extremely fast, but with finite speed. In this paper, we lift this assumption and explore the consequences of dealing with time-resolved data (finite speed of light), focusing on the relativistic effects that occur when the camera moves at speeds comparable with the speed of light.

Transient imaging has recently emerged as a vibrant, exciting area of research. Being able to analyze light transport at picosecond scale has already helped gain a better understanding of the complexities of light propagation [VWJ*12, VWJ*13], to approximate the shape of hidden objects [VWG*12] or reflectance properties of planar patches [NZV*11]. In this paper, we offer a novel contribution by visualizing relativistic effects of time-varying irradiance. Beyond the pure scientific interest of advancing the field of relativistic visualization, our work has direct applications in games (see for instance *OpenRelativity* from the MIT Game Lab [KTS13]) and education. Additionally, it can also help set the ground to derive a time-resolved theory of light transport.

Relativistic rendering is not new [CLC96, WBE*06]. However, our time-resolved framework implies by definition that surface irradiance is not constant in the temporal domain, so existing models must be revised and redefined. We describe here our technique to render and inspect scenes where relativistic effects take place: in particular, we address time dilation, light aberration, the Doppler effect and the searchlight effect. Moreover, no existing model of relativistic rotation exists in the literature, which hinders free exploration of scenes; we additionally introduce the first model of relativistic sensor rotation in computer graphics.

To obtain input data, we rely on two sources of information. One the one hand, the recent imaging technique by Velten and colleagues called *femto-photography* [VWJ*13]. Guided by a femto-second laser as a light source, it has an effective exposure time per frame of less than 2 ps, allowing to visualize the *propagation* of light through a scene. This is real-world captured data, which we leverage using image-based rendering techniques. Since the camera cannot be moved in Velten's setup (please refer to Section 3 and the original paper for more details), our technique allows to visualize novel view points, synthesizing light transport in a physically accurate manner. On the other hand, we also employ the transient renderer by Jarabo et al. [JMG13], which allows us to create novel scenes and render simulations of time-resolved light transport. Both approaches can help gain a deeper understanding of light transport at picosecond scale.

In summary, we have developed a rendering and visualization tool for transient light transport, capable of simulat-

ing generalized relativistic effects, freed from the restrictions of previous works. Our contributions can be summarized as follows:

- We revise and correct well-established concepts about relativistic rendering, to take into account that irradiance can no longer be assumed to be constant over time
- Previous techniques were also limited by linear velocities of the (virtual) cameras. We propose the first approximate solution for the case of a *rotating* sensor, so the camera can be freely moved in 3D space
- We implement a fully working prototype, which allows interactive visualization and exploration of both real and simulated data

2. Related Work

Time Resolved Light Transport A modified rendering equation can account for the finite speed of light and handle transient effects [Arv93, SSD08]. However, in previous works no practical rendering framework is derived from the proposed transient rendering framework. A fully functional time-resolved rendering system was recently presented by Jarabo and colleagues [JMG13]. Wu et al. [WWB*12] perform a rigorous analysis on transient light transport in frequency space. They derive an analytic expression that models the information transfer between dimensions, and show that this derivation can be exploited to build a bare-sensor imaging system.

Time-resolved imaging is further analyzed by Wu et al. [WOV*12] to separate direct and global illumination components in macroscopic table-top scenes. The authors analyze the time profile for each pixel and decompose it into direct, subsurface scattering and interreflection components. Kirmani et al. [KHDR09] utilized global information in time-of-flight images to infer geometries of hidden objects, not directly visible by the camera, by using the encoded time-of-flight of diffuse indirect illumination. This work was further improved by Velten et al. [VWG*12]. Material BRDFs of distant patches were reconstructed [NZV*11] via light-bounce analysis from ultrafast image measurements.

Last, Velten et al. [VWJ*12, VWJ*13] developed *femto-photography*, a technique that allows ultra-fast (in the order of picoseconds) capture of transient light transport, by using a streak sensor, a femto-second laser, and computational techniques. We explain this system in more detail in Section 3, since we rely on the data it provides to render some of the relativistic effects shown in this paper. This femto-photography technique has inspired new approaches in transient imaging: recently, Heide et al. [HHGH13] developed a system based on photonic mixer devices. While the hardware employed is cheaper, the temporal resolution is not as good, and the system relies on heavy optimization which can take several hours.

Relativistic Rendering Here we discuss the most relevant work on relativistic rendering. For a wider survey, we refer to [WBE*06], where the different proposed techniques for both general and special relativistic rendering are discussed, including their application as educational tools. Chang et al. [CLC96] introduced the theory of Special Relativity in the field of computer graphics. Their work accounts for geometric and radiance transformations due to fast moving objects or camera. However, their formulation modeled the searchlight and Doppler effects incorrectly; these were later corrected by Weiskopf et al. [WKR99]. Following work [WKR00] simulates relativistic effects in real captured scenes modeled with image-based techniques, by applying the relativistic transformations directly on the light field. However, the authors assume light incoming from infinitely far away light sources with constant radiance, so both the effects of distance and time-varying irradiance are ignored. This allows them to make some simplifying assumptions about the radiance in the scene, which no longer hold in the context of time-resolved data we deal with. Finally, visualization approaches and games have been created with a didactic goal, aiming at helping students in the understanding of relativity. The game *A Slower Speed of Light*, notable among these, uses the open-source toolkit *OpenRelativity* which works with the *Unity* engine and can simulate special relativity effects [KTS13]. However, to our knowledge, they do not deal with time-varying irradiance either.

3. Time-Resolved Data

In this section we introduce briefly our two sources of time-resolved light transport data: the novel femto-photography technique of Velten et al. [VWJ*13] allows us to capture real data, while the rendering system of Jarabo at el. [JMG13] provides simulated results. Note that Velten et al.'s paper describes the capture setup, while this work deals with synthesizing new viewpoints based on the captured data, and taking into account the associated relativistic effects that arise. We refer the reader to the original references for more details.

3.1. Femto-Photography

The term femto-photography [VWJ*12, VWJ*13] refers to a novel imaging technique which allows to code time of arrival of individual photons on a spatial coordinate of a regular sensor. The technique has an effective exposure time of down to 1.85 picoseconds, which allows to image the propagation of light as it interacts with objects in a scene, opening up new and exciting possibilities in forward and inverse light transport analysis.

The system works as follows (see Figure 1 for a schematic overview): a *Ti:Sapphire* femto-second laser pulse is repeatedly shot against a diffuser, which reflects it into the scene as a spherical wave. Light interacts with the scene, and photons enter the camera through a horizontal slit (thus only a single scan line is imaged at a time). Within the camera, which

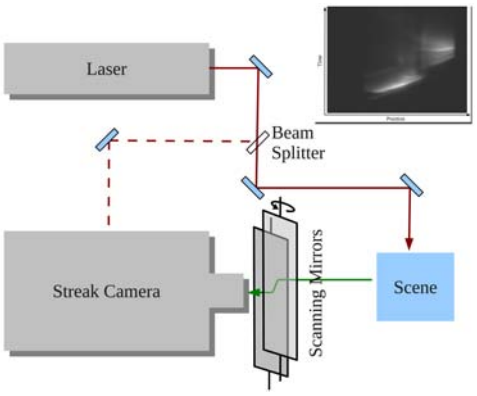

Figure 1: *Schematic view of the* femto-photography *setup. The inset shows an example streak image, as captured by the sensor. The streak camera encodes time of arrival of individual photons in the y-dimension by means of a time-varying voltage.*

is known as a *streak camera* and is synchronized with the laser pulse by means of a beam splitter, photons are converted into electrons and then deflected vertically by a time-varying voltage. In this way, photons arriving first will be imaged onto different parts of the sensor along its vertical coordinate, effectively coding time as a spatial coordinate in the sensor. This yields one x-t *streak image* (see the inset in Figure 1). A rotating mirror progressively scans the whole scene along its y-coordinate, as more laser pulses are shot. This generates a 3D volume of x-y-t time-resolved data which, when visualized along the t coordinate, produces the final videos[†].

3.2. Transient Rendering

Jarabo et al. [JMG13] build over the classical rendering equation, by introducing the time domain:

$$\begin{aligned} L(x,\omega_o,t) &= L_e(x,\omega_o,t) \\ &+ \int_{\Omega^+} L_i(x,\omega_i,t)\rho(x,\omega_i,\omega_o)(-\omega_i\cdot n)d\omega_i \end{aligned} \quad (1)$$

where x is the point in the scene being illuminated, n its normal; ω_i and ω_o the incoming and outgoing directions, respectively; $L_e(x,\omega_o,t)$ is the emitted radiance in direction ω_o at time instant t; $L_i(x,\omega_i,t)$ is the incoming radiance at x from direction ω_i at instant t; $\rho(x,\omega_i,\omega_o)$ represents the BRDF at x; and Ω^+ is the hemisphere centered at n. The solution to this equation is computed by Montecarlo ray tracing, taking into account the distance traveled by a ray from its origin to the next intersection, as well as the index of refraction η of the medium. This affects the speed of light v in the medium according to the equation $v = c/\eta$, where c is the speed of light in a vacuum.

Figure 2 shows some results for the *bunny* scene. A spherical wavefront of light advances towards the bunny inside a Cornell box. The first two frames show the primary wavefront reaching the floor, the bunny and the left wall, while some secondary fronts reflecting from the bunny appear on the floor. The front on the left wall appears mostly white due to dynamic range issues, since the primary waveform has much more energy than the secondary reflections. The third and fourth frames show the primary wavefront past the bunny and reaching the farthest wall, plus the rich combination of multiple reflections.

4. Relativistic Rendering

Time-resolved data allows us to explore light transport like never before, no longer being constrained by the assumption that light speed is infinite. While this is indeed a valid assumption in most cases, the possibilities that open up analyzing the dynamics of light at pico-second resolution are fascinating.

4.1. Frames of Reference

Assuming that the geometry in the scene is known (which can be easily acquired with a digitizer arm or from time-of-flight data), we can synthesize new viewpoints and animations of the scene by taking an image-based rendering approach, using x-y textures from the x-y-t data cube and projecting them onto the geometry. This allows us to visualize real-world events from new, interesting angles. However, visualizing light transport events at this time scale yields counter-intuitive results, as observed by Velten et al. [VWJ*13]. Due to the finite speed of light, events are not captured in the sensor as they occur, which leads to unexpected apparent distortions in the propagation of light. Figure 3 illustrates this. From this observation, it follows that two different temporal frames of reference must be employed: one for the world (when the events occur) and one for the camera (when the events are actually captured).

As a consequence, sensor data acquired by the femto-photography technique appears *warped* in the temporal domain, and must be *time-unwarped* to take into account the finite speed of light. So for each frame in the synthesized animations, we access the original warped data and apply the following transformation [VWJ*13]:

$$t'_{ij} = t_{ij} + \frac{z_{ij}}{c/\eta} \quad (2)$$

where t'_{ij} and t_{ij} are camera and world times respectively, z_{ij} is the depth from each point (i,j) to the new camera position, and η the index of refraction of the medium. Note how a naive approach based on simply sticking the textures from the first frame to the geometry through the animation

[†] Videos and data from scenes captured with this setup can be found online at: http://femtophotography.info

Figure 2: *The first four images show selected frames of a time-resolved rendering for the bunny scene [JMG13]. The rightmost image shows the classic view of the scene, with all light integrated on the sensor during the simulated exposure.*

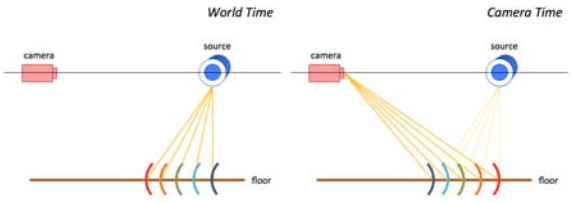

Figure 3: *Counter-intuitive results in time-resolved imaging. Left: photons are shot simultaneously from the light source towards the floor. Because their traveled distances are different, they reach the floor at slightly different times, and a wavefront appears traveling right to left (color-coded blue to red). Right: Since the distances to the sensor are also different, the bounced photons reach the sensor in inverse order. The result is that the wavefront imaged on the sensor travels in the reverse direction, left to right.*

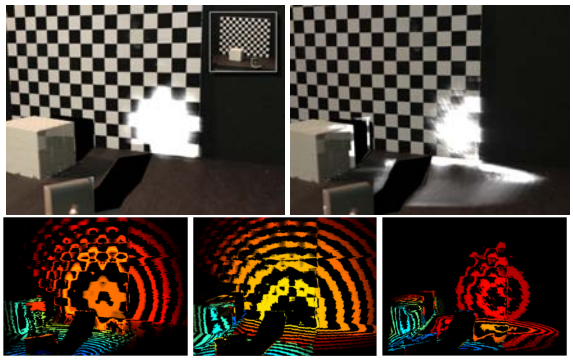

Figure 4: *Time unwarping between camera time and world time for synthesized new views of a cube scene. Top row, left: Scene rendered from a novel view keeping the unwarped camera time from the first frame (the small inset shows the original viewpoint). Right: The same view, warping data according to the new camera position. Notice the large changes in light propagation, in particular the wavefronts on the floor not visible in the previous image. Bottom row: Isochrones visualization of the cube-scene for a given virtual camera (color encodes time); from left to right: original x-y-t volume in the time-frame of the capturing camera, unwarped x-y-t data in world time frame, and re-warped data for the new virtual camera. Note the striking differences between corresponding isochrones.*

would produce wrong results; the distance from each geometry point to the center of projection of the camera varies for each frame, and thus a *different* transformation must be applied each time to the original, *warped* x-y-t data (see Figure 4). We assume a pinhole model for the camera.

4.2. Relativistic Effects

Apart from the time-warping of data, macroscopic camera movement at pico-second time scales, like the one synthesized in Figure 4 would give rise to relativistic effects. This requires a relativistic framework to correctly represent and visualize light traveling through the 3D scene. Although simulations of relativistic effects have existed for a while [CLC96, WBE*06], visualizing our particular time-resolved datasets requires departing from the common simplifying assumption of constant irradiance on surfaces. As we will see in the following paragraphs, this has direct implications on how radiance gets imaged onto the sensor.

According to special relativity, light aberration, the Doppler effect, and the searchlight effect need to be taken into account when simulating motion at fast speeds. *Light aberration* accounts for the apparent geometry deformation caused by two space-time events measured in two reference frames moving at relativistic speeds with respect to each other. The *Doppler effect* produces a wavelength shift given by the Doppler factor. Last, the *searchlight effect* increases or decreases radiance, according to whether the observer is approaching or moving away from a scene. We modify existing models for the three effects to support time-resolved irradiance, and approximate the yet-unsolved solution for camera rotation.

We build our relativistic visualization framework on the derivations by Weiskopf et al. [WKR99]. We consider two inertial frames, O and O', where O' (the sensor) is moving with velocity $v = \beta c$ with respect to O, with $\beta \in [0..\pm 1)$.

L represents radiance measured in O, defined by direction (θ,ϕ) (defined with respect to the motion direction) and wavelength λ. The corresponding primed variables (θ',ϕ') and λ' define radiance L' measured in O'. To obtain the modified radiance L' given L and the speed of the sensor, we need to apply the following equation:

$$L'(\theta',\phi',\lambda') = D^{-5} L\left(arccos\frac{cos\theta'+\beta}{1+\beta cos\theta'},\phi',\frac{\lambda'}{D}\right) \quad (3)$$

where $D=\gamma(1+\beta cos\theta')$ and $\gamma = 1/\sqrt{1-\beta^2}$. This equation accounts for all three factors: light aberration, the Doppler effect, and the searchlight effect. However, it cannot model explicitly the effect of special relativity on time-resolved irradiance. In the following paragraphs we explain each effect separately, and discuss the modifications needed to handle time-resolved irradiance.

Time dilation: Breaking the assumption of constant irradiance means that we cannot ignore the effect of time dilation [Ein61]. Time dilation relates directly with Lorentz contraction, and is defined as the difference in elapsed time Δt between two events observed in different inertial frames; for our world and camera frames of reference, this translates into $\Delta t' = \gamma \Delta t$. This means that time in these two frames advances at different speeds, making time in the stationary frame (the world) advance faster than in the moving frame (the camera). Thus, we need to keep track of both world t and camera time t', since they differ depending on the motion speed.

Light aberration: An easy example to understand light aberration is to visualize how we see rain drops when traveling on a speeding train. When the train is not moving, raindrops fall vertically; but as the train picks up speed, raindrop trajectories become increasingly diagonal as a function of the train's speed. This is because the speed of the train is comparable with the speed of raindrops. A similar phenomenon occurs with light if moving at relativistic speeds. However, as opposed to rain drops, relativistic light aberration cannot be modeled with classical physics aberration; the Lorentz transformation needs to be applied instead.

Light aberration is computed by transforming θ' and ϕ' with the following equations, which provide the geometric transformation between two space-time events measured in two reference frames which move at relativistic speeds with respect to each other:

$$cos\theta' = \frac{cos\theta-\beta}{1-\beta cos\theta} \quad (4)$$

$$\phi' = \phi \quad (5)$$

The end result is that light rays appear curved, with more curvature as velocity increases. Given this curvature, light rays reaching the sensor from behind the camera become visible. Finally, as β approaches 1, and thus $v \approx c$, most incoming light rays are compressed towards the motion direction; this makes the scene collapse into a single point as the camera moves towards it (note that this produces the wrong impression that the camera is moving *away* from the scene). The first two rows in Figure 5 show the effects of light aberration with increasing velocity as the sensor moves at relativistic speeds, towards and away from the scene respectively.

Doppler effect: The Doppler effect is better known for sound, and it is not a phenomenon restricted to relativistic velocities. In our case, the Doppler effect alters the observed frequency of the captured events in the world when seen by a fast-moving camera, which produces a wavelength shift, as defined by the Doppler factor D:

$$\lambda' = D\lambda \quad (6)$$

The overall result is a color shift as a function of the velocity of the sensor relative to the scene. Somewhat less known, the Doppler effect also creates a perceived speed-up (or down, depending on the direction of camera motion) of the captured events. This means that the *frame rate* of the time-varying irradiance f in world frame is Doppler shifted, making the perceived frame rate f' in camera frame become $f' = f/D$. Figure 5 (third row) shows an example of the Doppler effect.

Searchlight effect: Due to the searchlight effect, photons from several instants are captured at the same time differential, in part as a cause of the Doppler shift on the camera's perceived frame rate. This results in increased (if the observer is approaching the scene) or decreased (if the observer is moving away) brightness (see Figure 5, bottom row):

$$L'(\theta',\phi',\lambda') = D^{-5} L(\theta,\phi,\lambda) \quad (7)$$

Intuitively, continuing with our previous rain analogy, it is similar to what occurs in a vehicle driving in the rain: the front windshield will accumulate more water than the rear windshield. For our time-varying streak-data, this means that irradiance from several *frames* in world time interval dt is integrated over the same camera differential time dt', such that $dt = dt'/D$. Note that the D^{-5} factor only is valid for the case in which the directions of the velocity vector v and the normal to the detector are parallel. We later show how to approximate a rotation of the sensor.

Finally, Figures 6 and 7 show the result of combining all these relativistic effects, both for the *cube* scene (data captured with femto-photography techniques) and the *bunny* scene (simulated data by rendering) respectively. The laser wavelength is set at 670 nm for visualization purposes. We refer the reader to the supplementary videos to see the full animations.

4.3. Relativistic Rotation

Providing free navigation of a scene depicting time-resolved light transport implies that the viewers should be allowed to rotate the camera. However, there is no universally accepted

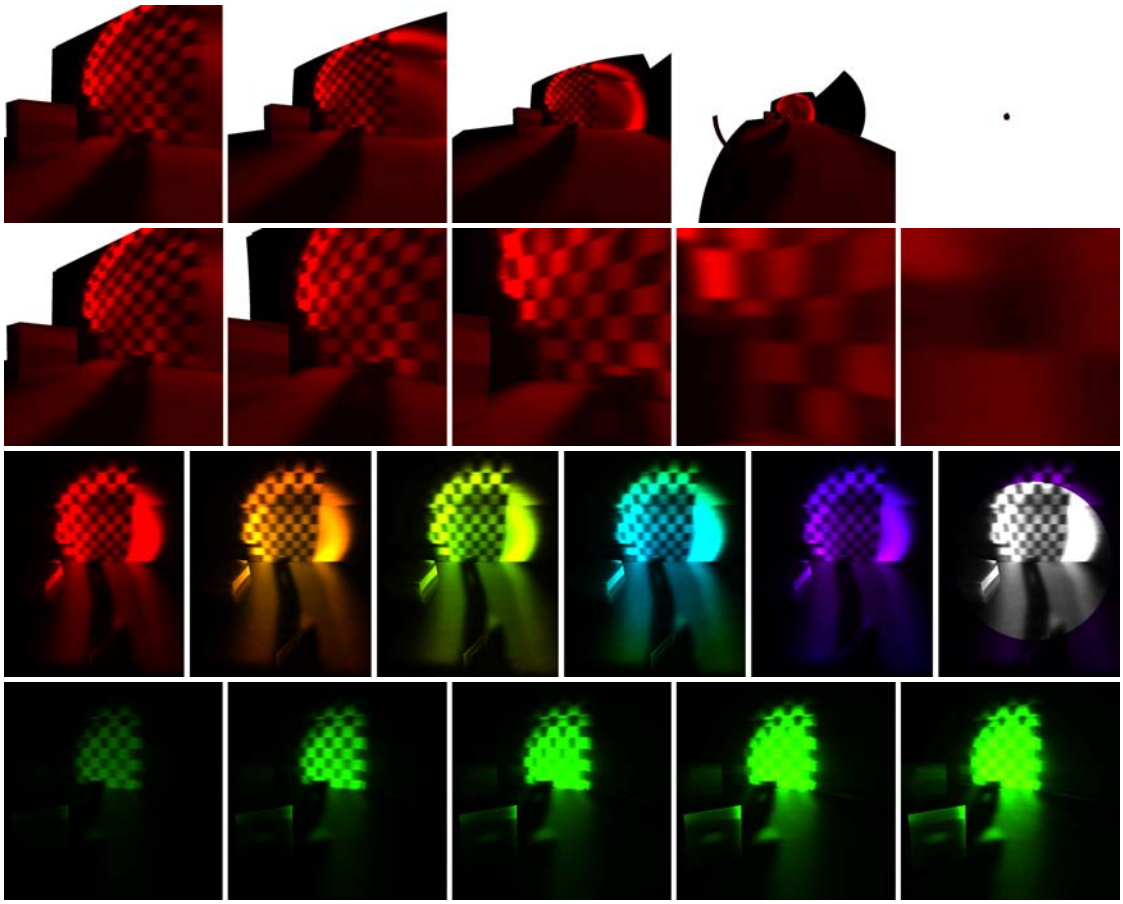

Figure 5: *Relativistic effects shown separately for the cube scene. First row: Distortion due to light aberration as the camera moves towards the scene at different velocities, with* $\beta = \{0, 0.3, 0.6, 0.9, 0.99\}$. *We assume a laser wavelength of 670 nm for visualization purposes. Second row: The same effect as the sensor moves away from the scene, with the opposite velocity from the previous row. Notice how in both cases light aberration produces counter-intuitive results as the camera appears to be moving in the opposite direction. Third row: Doppler effect, showing the shift in color as a consequence of the frequency shift of light reaching the sensor, with* $\beta = \{0, 0.15, 0.25, 0.35, 0.50, 0.55\}$. *Fourth row: Searchlight effect, resulting in an apparent increase in brightness as the speed of the approaching camera increases, with* $\beta = \{0, 0.2, 0.3, 0.4, 0.5\}$ *(simulated laser at 508 nm). All images have been tone-mapped to avoid saturation.*

theory of relativistic rotation [RR04]. We propose a suitable approximation based on limiting the rotation to very small angles per frame, so the differential rotation of the camera's viewing direction between frames can be neglected. However, for non-infinitesimal sensors this small rotation causes that the sensor's differential surfaces to move at different speeds: it creates a continuous linear velocity field Ψ on the sensor, with a zero-crossing at the axis of rotation.

To simulate the rotation of the camera we therefore first divide the sensor S in different areas $s \in S$. Our approximation effectively turns each of them into a different translational frame, with linear velocity ψ_s. Then, for each s we render the scene applying the novel relativistic transformations introduced in this section, with a different β_s for each s (trivially obtained from an input β measured at the edge of the sensor). This makes the incoming radiance be deformed differently depending on the position of the sensor where it is imaged. Figure 8 shows an example, where the sensor is rotating clockwise.

5. Implementation

Our implementation allows for real-time visualization of relativistic effects, both from real and simulated data. It is implemented in OpenGL as an stand-alone application, taking as input the reconstructed geometry of the scene, as well as the time-resolved data. The system is based on classic

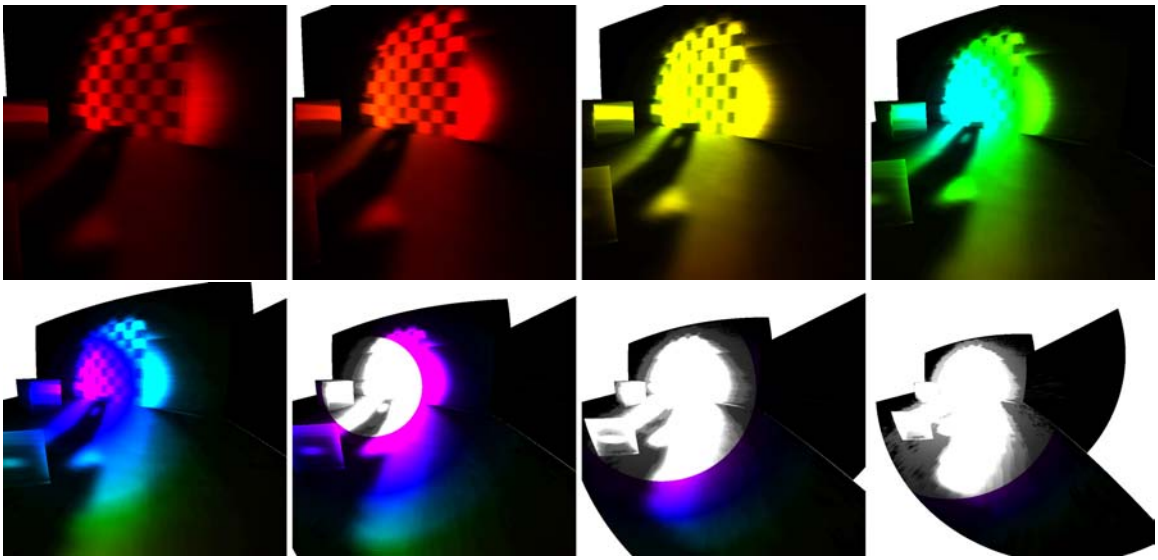

Figure 6: *Relativistic phenomena for the cube scene (real data) including light aberration, Doppler effect and the searchlight effect, as the camera approaches the scene at increasing relativistic velocities $v = \beta c$ (with β increasing from 0 to 0.77).*

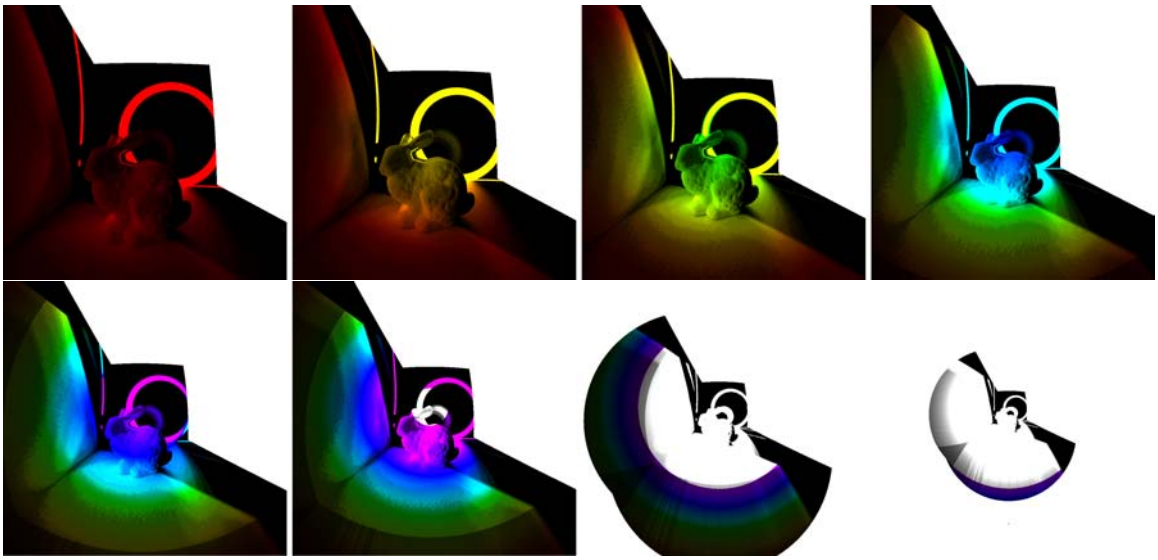

Figure 7: *Relativistic phenomena for the bunny scene (simulated data) including light aberration, Doppler effect and the searchlight effect, as the camera approaches the scene at increasing relativistic velocities $v = \beta c$ (with β increasing from 0.2 to 0.9). Note that we transform the RGB computed radiance into luminance.*

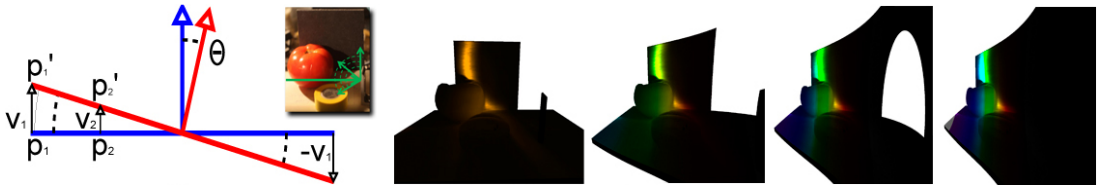

Figure 8: *Relativistic rotation. Left: assuming that the rotation angle θ can be neglected between frames, we model the rotation as a continuous linear velocity field on the sensor Ψ, so each differential area is assigned a different velocity ψ_s. This causes that depending on the position on the sensor, different relativistic transformations are applied on the scene. The rest of the frames show the effects of a clockwise rotation of the sensor, with $\beta = \{0, 0.4, 0.8, 0.99\}$ (measured at the edge of the sensor). The small inset shows the original scene.*

image-based rendering (IBR) techniques, where the shading of the surface is modeled by the images projected over the surface.

In our case, we use x-y images from the x-y-t data cube to shade the geometry. The cube is stored as a 3D texture on the GPU in *world time* coordinates. This allows us to apply time-warping to adapt it to the new viewpoint in rendering time, by simply applying the transformation defined in Equation 2 (see Section 4.2).

Due to light aberration the geometry viewed from the camera is distorted. This distortion causes straight lines to become curved, so the geometry has to be re-tessellated. Image-space warping, which has been used in many scenarios [CSHD11, TDR*12, MWA*13] and may appear as an alternative, is not viable in this scenario because of the large extent of the deformations, that make well-known problems of warping such as disocclusions clearly apparent. Our implementation performs the re-tessellation off-line on the CPU, but it is straightforward to tessellate it on the GPU on the fly. Then, in render time, each vertex should be transformed according to Equation 3.

Doppler effect is introduced by modifying the wavelength of the outgoing illumination from the surfaces. To avoid the complexity of a full-fledged spectral renderer, we assume light with energy in only one wavelength of the spectrum. To display radiance we use a simple *wavelenght-to-RGB* conversion encoded as a 1D texture. Wavelengths out of the visible spectrum are displayed as gray-scale values.

Finally, when modeling the searchlight effect, we avoid the straightforward approach to access all frames in the streak data cube, bounded by dt, and integrate them. This would require several accesses to the 3D texture, which would hinder interactivity. Instead, we pre-integrate irradiance values in the temporal domain, and use anisotropic mipmapping to access the pre-integrated irradiance values, using dt to select the mipmap level in the time dimension.

6. Conclusions and Future Work

In this paper we visualize light transport effects from an entirely new perspective, no longer constrained by the assumption of infinite speed of light. We hope this will spur future research and help to better understand the complex behavior of time-resolved interactions between light and matter. We have used real data from the recent femto-photography technique [VWJ*13], as well simulation data produced by a physically-based ray tracing engine especially designed to support transient rendering [JMG13].

To visualize this data, we have developed an interactive image-based rendering application, that allows free navigation through the reconstruction of the captured scenes, including physically-based relativistic effects due to fast camera motion. We have introduced, for the first time in computer graphics, the modified equations necessary to render surfaces when irradiance is not constant over time, as well as an approximate solution for the case of rotation, for which a definite solution does not exist in the physics literature.

Of course there is plenty of exciting future work ahead. Our current implementation assumes Lambertian surfaces, so the viewing angle with respect to the normal has no influence in the result. This assumption can be relaxed by using more sophisticated IBR techniques e.g. [BG01]. Additionally, right now we only use radiance as captured by the sensor. When camera movement reveals surfaces which were originally occluded, we simply render them black. However, the use of time-resolved photographic techniques has already demonstrated promising results at recovering hidden information, including both geometry [VWG*12] and a parametric model of reflectance [NZV*11]. A promising avenue of research we are already working on involves generalizing these seminal works to be able to obtain both geometry and reflectance at the same time for hidden objects.

Acknowledgements

This research has been funded by the European Commission, Seventh Framework Programme, through the projects GOLEM (Marie Curie IAPP, grant agreement no.: 251415) and VERVE (Information and Communication Technologies, grant agreement no.: 288914), the Spanish Ministry of Science and Technology (TIN2010-21543), by the Media Lab Consortium Members, MIT Lincoln Labs and the Army Research Office through the Institute for Soldier Nanotechnologies at MIT. Belen Masia was additionally funded by an FPU grant from the Spanish Ministry of Education and by an NVIDIA Graduate Fellowship. Ramesh Raskar was supported by an Alfred P. Sloan Research Fellowship and a DARPA Young Faculty Award.

References

[Arv93] ARVO J.: Transfer equations in global illumination. In *Global Illumination, SIGGRAPH'93 Course Notes* (1993). 2

[BG01] BOIVIN S., GAGALOWICZ A.: Image-based rendering of diffuse, specular and glossy surfaces from a single image. In *Proceedings of the 28th annual conference on Computer graphics and interactive techniques* (2001), SIGGRAPH '01, pp. 107–116. 8

[CLC96] CHANG M.-C., LAI F., CHEN W.-C.: Image shading taking into account relativistic effects. *ACM Trans. Graph. 15*, 4 (Oct. 1996), 265–300. 1, 2, 4

[CSHD11] CHAURASIA G., SORKINE-HORNUNG O., DRETTAKIS G.: Silhouette-aware warping for image-based rendering. *Computer Graphics Forum (Proceedings of the Eurographics Symposium on Rendering) 30*, 4 (2011). 8

[Ein61] EINSTEIN A.: *Relativity: the special and the general theory*. Crown Publishers, 1961. 5

[GNJJ08] GUTIERREZ D., NARASIMHAN S., JENSEN H., JAROSZ W.: Scattering. In *ACM SIGGRAPH Asia Courses, 18* (2008). 1

[HHGH13] HEIDE F., HULLIN M., GREGSON J., HEIDRICH W.: Low-budget transient imaging using photonic mixer devices. *ACM Trans. Graph. 32*, 4 (2013). 2

[JMG13] JARABO A., MASIA B., GUTIERREZ D.: *Transient Rendering and Relativistic Visualization*. Tech. Rep. TR-01-2013, Universidad de Zaragoza, April 2013. 1, 2, 3, 4, 8

[KHDR09] KIRMANI A., HUTCHISON T., DAVIS J., RASKAR R.: Looking around the corner using transient imaging. In *ICCV* (2009). 2

[KTS13] KORTEMEYER G., TAN P., SCHIRRA S.: A slower speed of light: Developing intuition about special relativity with games. In *Proceedings of the International Conference on the Foundations of Digital Games (FDG)* (2013). 1, 2

[MWA*13] MASIA B., WETZSTEIN G., ALIAGA C., RASKAR R., GUTIERREZ D.: Display adaptive 3D content remapping. *Computers & Graphics* (2013). 8

[NZV*11] NAIK N., ZHAO S., VELTEN A., RASKAR R., BALA K.: Single view reflectance capture using multiplexed scattering and time-of-flight imaging. *ACM Trans. Graph. 30* (Dec. 2011), 171:1–171:10. 1, 2, 8

[RR04] RIZZI G., RUGGIERO M. L.: *Relativity in Rotating Frames*. Kluber Academic, 2004. 6

[SSD08] SMITH A., SKORUPSKI J., DAVIS J.: *Transient Rendering*. Tech. Rep. UCSC-SOE-08-26, School of Engineering, University of California, Santa Cruz, February 2008. 2

[TDR*12] TEMPLIN K., DIDYK P., RITSCHEL T., MYSZKOWSKI K., SEIDEL H.-P.: Highlight microdisparity for improved gloss depiction. *ACM Trans. Graph. 31*, 4 (July 2012), 92:1–92:5. 8

[VWG*12] VELTEN A., WILLWACHER T., GUPTA O., VEERARAGHAVAN A., BAWENDI M. G., RASKAR R.: Recovering three-dimensional shape around a corner using ultrafast time-of-flight imaging. *Nature Communications*, 3 (July 2012). 1, 2, 8

[VWJ*12] VELTEN A., WU D., JARABO A., MASIA B., BARSI C., LAWSON E., JOSHI C., GUTIERREZ D., BAWENDI M. G., RASKAR R.: Relativistic ultrafast rendering using time-of-flight imaging. In *ACM SIGGRAPH 2012 Talks* (2012). 1, 2

[VWJ*13] VELTEN A., WU D., JARABO A., MASIA B., BARSI C., JOSHI C., LAWSON E., BAWENDI M., GUTIERREZ D., RASKAR R.: Femto-photography: Capturing and visualizing the propagation of light. *ACM Trans. Graph. 32*, 4 (2013). 1, 2, 3, 8

[WBE*06] WEISKOPF D., BORCHERS M., ERTL T., FALK M., FECHTIG O., FRANK R., GRAVE F., KING A., KRAUS U., MULLER T., NOLLERT H.-P., RICA MENDEZ I., RUDER H., SCHAFHITZEL T., SCHAR S., ZAHN C., ZATLOUKAL M.: Explanatory and illustrative visualization of special and general relativity. *IEEE Transactions on Visualization and Computer Graphics 12*, 4 (July 2006), 522–534. 1, 2, 4

[WKR99] WEISKOPF D., KRAUS U., RUDER H.: Searchlight and doppler effects in the visualization of special relativity: A corrected derivation of the transformation of radiance. *ACM Trans. Graph. 18*, 3 (1999). 2, 4

[WKR00] WEISKOPF D., KOBRAS D., RUDER H.: Real-world relativity: Image-based special relativistic visualization. In *IEEE Visualization* (2000), pp. 303–310. 2

[WOV*12] WU D., O'TOOLE M., VELTEN A., AGRAWAL A., RASKAR R.: Decomposing global light transport using time of flight imaging. In *IEEE Computer Vision and Pattern Recognition* (2012), pp. 366 –373. 2

[WWB*12] WU D., WETZSTEIN G., BARSI C., WILLWACHER T., O'TOOLE M., NAIK N., DAI Q., KUTULAKOS K., RASKAR R.: Frequency Analysis of Transient Light Transport with Applications in Bare Sensor Imaging. In *European Conference on Computer Vision 2012* (2012). 2